



SERS based determination of ceftriaxone, ampicillin, and vancomycin in serum using WS₂/Au@Ag nanocomposites and a 2D-CNN regression model

Ying Cao ^a, Yuxin Yang ^a, Wendong Zhao ^a, Hongyi Liu ^a, Xuedian Zhang ^a, Hui Chen ^a, Mingxing Sui ^b, Pei Ma ^{a,*}

^a Key Laboratory of Optical Technology and Instrument for Medicine, Ministry of Education, College of Optical-Electrical and Computer Engineering, University of Shanghai for Science and Technology, Shanghai 200093 China

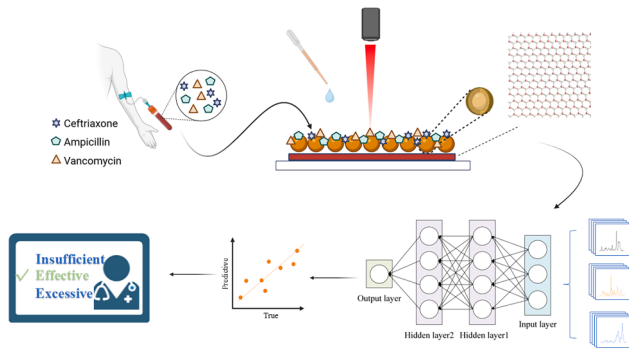
^b Department of Organ Transplantation, Shanghai Changhai Hospital, Shanghai 200433 China



HIGHLIGHTS

- SERS was employed to characterize three commonly used antibiotics: ceftriaxone, ampicillin, and vancomycin.
- WS₂/Au@Ag nanocomposites were developed as SERS substrates, and a detection limit of 10⁻¹⁴ M was achieved for R6G.
- The concentrations of antibiotics were predicted using a 2D-CNN deep learning model.
- The prediction performance was improved by converting SERS spectroscopy data into 2D images through short-time Fourier transform.
- Deep learning-based SERS shows great promises in therapeutic drug monitoring.

GRAPHICAL ABSTRACT



ABSTRACT

Accurate therapeutic drug monitoring (TDM) of antibiotics including ceftriaxone, ampicillin, and vancomycin plays an important role in the treatment of neonatal sepsis, a common and life-threatening disease in neonates. A highly sensitive surface-enhanced Raman spectroscopy (SERS) method using tungsten disulfide/gold and silver core-shell (WS₂/Au@Ag) nanocomposites was developed for the rapid detection of the three antibiotics, with a wide response range (0.5–1000 µg/mL). A two-dimensional convolutional neural network (2D-CNN) regression model was proposed to predict antibiotic concentrations in complex mixed serum solutions, simulating various drug use scenarios. The model achieved excellent regression results for ceftriaxone and ampicillin simultaneously, with R-squared (R^2) values of 0.9993 and 0.9997. The integration of ultra-sensitive SERS with the 2D-CNN based deep learning model provides a promising approach for rapid TDM and personalized patient treatment.

1. Introduction

Neonatal sepsis remains a leading cause of hospitalization and death in newborns worldwide, affecting up to approximately 1 % live birth

[1]. *Escherichia coli* (*E. coli*) is one of the predominant pathogens that causes sepsis [2]. In the treatment of neonatal sepsis, ceftriaxone, ampicillin and vancomycin are the most common therapeutic agents. In clinic, before the results of blood cultures and other non-specific tests

* Corresponding author.

E-mail address: peima@usst.edu.cn (P. Ma).

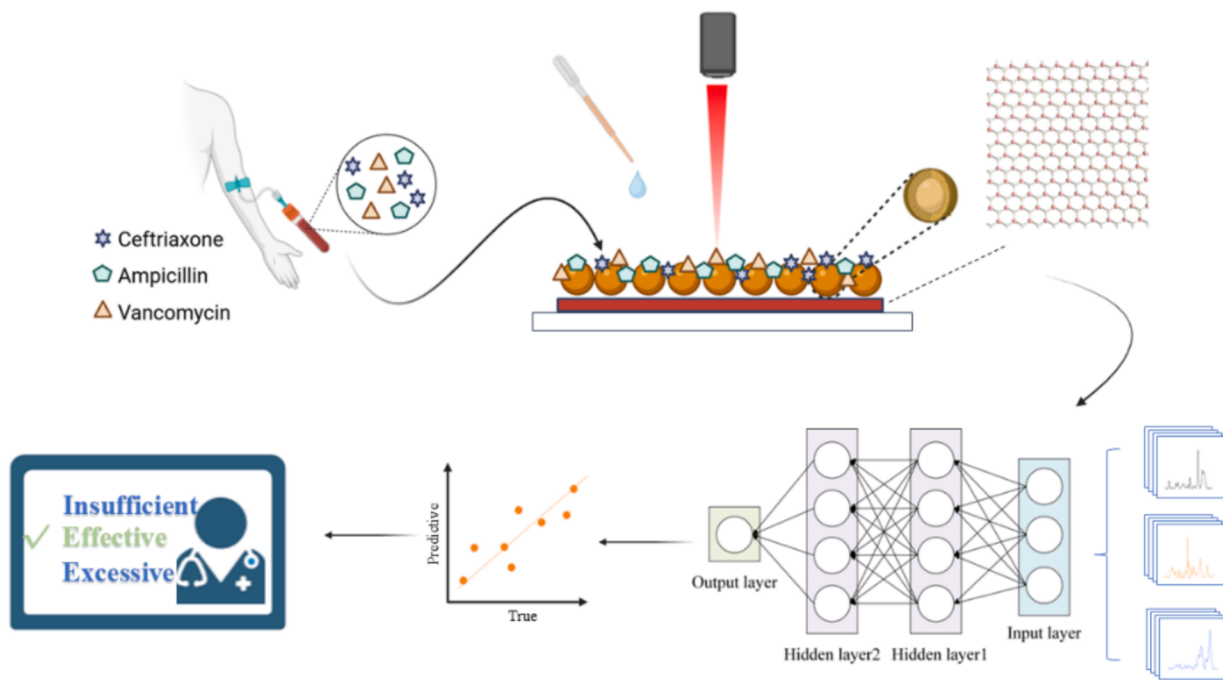


Fig. 1. Schematic diagram of antibiotic detection and analysis.

are available, a combination of broad-spectrum antimicrobial agents may be empirically used [3,4], such as ampicillin (or penicillin) plus a third-generation cephalosporin, to cover both Gram-positive (G+) and Gram-negative (G-) organisms [5].

The international guidelines for management of sepsis and septic shock have strongly suggested therapeutic drug monitoring (TDM) for the use of antibiotics in neonatal sepsis [6,7]. Ceftriaxone and ampicillin are common β -lactam antibiotics. During the treatment, underdose would fail to achieve adequate antimicrobial effect and prolong the use of antibiotics, as well as produce drug-resistant bacteria and shorten the service life of the drug. On the other hand, high concentrations will cause antibiotic abuse and toxicity, including neurotoxicity, hepatotoxicity, nephrotoxicity, and bone marrow suppression [8–10]. Vancomycin, a glycopeptide antibiotic with narrow therapeutic window and potential nephrotoxicity, has recommended therapeutic levels of 10.0–15.0 $\mu\text{g/mL}$ in neonate [11]. Previous studies have shown that TDM for vancomycin can significantly improve treatment efficacy and reduce the risk of nephrotoxicity [12]. TDM-based personalized dosing regimens have become a hot research topic and an important tool for controlling antibiotic overuse, reducing toxic side effects, and minimizing pathogen-induced drug resistance [7,13,14].

TDM is the process of quantitatively determining drug concentrations in a patient's body fluids. Subsequently, the clinical dosage is adjusted based on pharmacokinetic (PK) and pharmacodynamic (PD) principles, as well as the effective therapeutic window, to achieve personalized and precise medical care [15–17]. Antibiotics clear pathogens by achieving and maintaining certain concentrations at the site of infection. To effectively eliminate pathogens, an effective antibiotic concentration should be 4–8 times the minimum inhibitory concentration (MIC) [18]. Thus, measuring the drug concentration in the blood and compare it to the MIC can determine whether the concentration is within the therapeutic range, guiding subsequent dose adjustments. Currently, laboratories typically employ techniques such as high-performance liquid chromatography (HPLC), liquid chromatography-tandem mass spectrometry (LC-MS/MS), and immunoassays for TDM [17]. Immunoassays are traditional routine methods known for their short turnaround time, low cost and having commercial products. However, they may exhibit lower accuracy due to potential errors and

cross-reactivity with endogenous human antibodies and other biological components, leading to falsely elevated values. HPLC and LC-MS/MS offer higher sensitivity and resolution but are time-consuming, require expensive equipment and maintenance, and necessitate skilled personnel, making them challenging to implement on a large scale [17].

Surface-enhanced Raman spectroscopy (SERS), as a label-free technique, is recognized for its high sensitivity, selectivity and excellent biocompatibility [19–21], it is considered a powerful tool for the evaluation of complex chemical reactions and bioanalysis [22]. In recent years, SERS has been actively explored in TDM applications [23]. For example, narrow therapeutic window drugs, such as those with anti-tumor activity, like methotrexate (MTX) and 6-mercaptopurine (6-MP) [24–27]. At the same time, due to the nephrotoxicity, ototoxicity, and emergence of antibiotic resistance, the monitoring scope for antibiotics has also expanded, including nephrotoxic aminoglycosides and carbapenems [28–30]. The signal enhancement in SERS primary originates from "hot spots" in the substrate, where metal nanostructures generate enhanced regions through plasmonic resonance, enhancing the substrate's sensitivity. Over the past few years, transition metal dichalcogenides, especially molybdenum disulfide (MoS_2) and tungsten disulfide (WS_2), have been proposed as composite structures with metal–semiconductor materials, allowing for more uniform distribution of analytes and further enhancing the Raman enhancement effect [31,32]. The composite substrates are a combination of various kinds of resonance, addressing the defects of traditional noble metal substrates, such as high cost, poor uniformity, and lack of long-term stability and biocompatibility, and semiconductor substrates, such as the weak interaction between the semiconductor and molecules [33]. Existing studies have shown that this kind of composite substrates possess excellent adsorption properties and biocompatibility, exhibiting superior uniformity and Enhancement effect [34,35].

SERS also shows great promises for the quantification of drugs, especially with the help of rapidly developing deep learning techniques. SERS characteristic peaks and their intensity values contain information related to the molecular structure and chemical bond composition of a substance, which can be used to analyze and identify substances. For solution with a specific content, SERS intensities at characteristic peaks usually follow a linear regression, which is ideal for quantification.

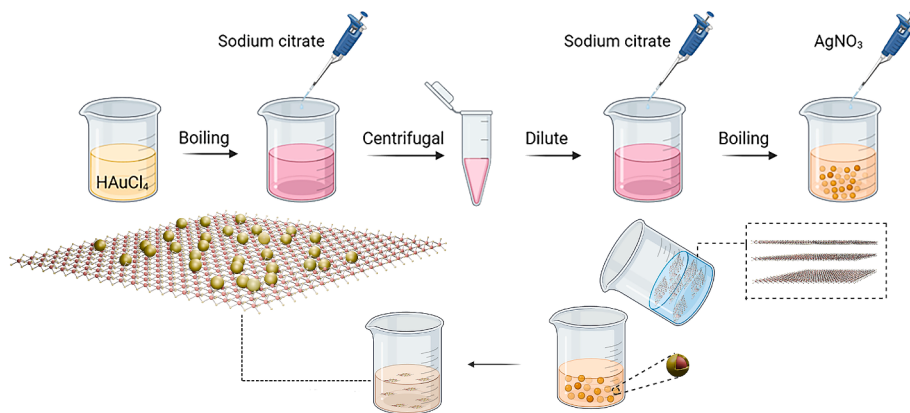


Fig. 2. Schematic diagram of WS₂/Au@Ag synthesis.

However, in the case of complex mixtures, SERS signals are susceptible to the competitive adsorption of the mixture components, such as other target molecules, proteins, and metabolic molecules in the solvent, which directly affects the reproducibility and sensitivity of SERS quantitative analysis [36–38]. Therefore, for solutions with multiple substances in complicated environments, the linear relationships would no longer be valid, and conventional methods cannot provide quantification results accurately. A more powerful tool is necessary to closely observe their subtle differences. Deep learning, with its automatic feature extraction, strong generalization, and robust big data processing capabilities, has achieved significant successes across various fields in both classification and regression tasks. Combining SERS with deep learning significantly enhances the efficiency and accuracy in handling complex factors and large datasets. This synergy has found critical applications in biomedical sciences, environmental protection, and food safety, providing improved detection and analytical capabilities. Several researchers have attempted to combine SERS spectroscopy with convolutional neural network (CNN) models to develop predictive models, such as for detecting zearalenone (ZEN) content in corn oil or the concentrations of lead ions and potassium sorbate in matsutake mushrooms. Whether predicting a single compound or multiple compounds, CNN models have demonstrated significant performance advantages [39,40]. Yuan *et al.* proposed combining a CNN model with the non-negative elastic net (NN-EN) algorithm, successfully predicting the proportions of individual components in mixed antibiotics after identifying the constituent antibiotics [41]. Although one-dimensional convolutional neural network (1D-CNN) combined with SERS spectral data has shown significant improvement than conventional methods, two-dimensional convolutional neural network (2D-CNN) has the potential to achieve better performance. CNN was originally designed for two-dimensional (2D) images, in which richer spatial structural information was provided, enhancing the feature extraction and identification in the model [42]. Multiple studies have shown that 2D-CNN achieved higher accuracy than 1D-CNN in classification tasks involving SERS spectral data of lung tissue, bladder cancer, and breast cancer [43–45]. 2D-CNN with near-infrared spectra has demonstrated ideal performance in predicting aflatoxins in moldy peanuts and detecting soil organic matter content [46,47]. Therefore, there is reason to believe that 2D-CNN combined with SERS have significant potential in addressing regression problems.

In this study, we have proposed a method utilizing SERS to qualitatively and quantitatively determine the content of ceftriaxone, ampicillin, and vancomycin in blood (Fig. 1). Firstly, a hybrid tungsten disulfide/gold and silver core-shell (WS₂/Au@Ag) nanoparticle substrate was developed for SERS detection. Secondly, the SERS spectra of three antibiotic drugs were acquired with a rapid, convenient and economic method. The spectra well matched their structure, and representative characteristic peaks were selected for quantitative analysis (1353 cm⁻¹ for ceftriaxone, 1000 cm⁻¹ for ampicillin, and 1594 cm⁻¹

for vancomycin, respectively). For each drug, a linear response was characterized between the SERS intensity and drug concentration from 0.5 µg/mL to 1000 µg/mL. Finally, to simulate the clinical scenario of combination therapy, a 2D-CNN deep learning algorithm was proposed to predict the concentrations of mixed ceftriaxone and ampicillin in serum. This will provide guidance on TDM in more complicated situations and help with drug dosage determination in clinic. The proposed method was highly sensitive, easy to operate, and holds promise for providing rapid, convenient, and accurate TDM for common treatment drugs in neonatal sepsis, supporting personalized treatment regimens with data-driven insights.

2. Materials and methods

2.1. Reagents

Chloroauric acid tetrahydrate (HauCl₄·4H₂O), sodium citrate dihydrate (C₆H₅Na₃O₇·2H₂O ≥ 899.0 %), silver nitrate solution (AgNO₃), ceftriaxone, ampicillin and vancomycin were purchased from MACKLIN (Shanghai, China). Fetal bovine serum (FBS, 10 %) was obtained from Hangzhou Sijiqing Biological Engineering Materials Co., Ltd. WS₂ dispersion was obtained from Nanjing Tanxun Nanomaterials Technology Co., Ltd. All subsequent experiments were conducted using deionized water with a resistivity of 18.25 MΩ.

2.2. WS₂/Au@Ag synthesis and characterization

The synthesis of the nanomaterials was carried out on a class 100 clean bench (SX-BHC, SuXin, China). The preparation of the WS₂/Au@Ag core-shell nanostructures involved two steps, as illustrated in Fig. 2. The first step was to synthesize gold and silver core-shell (Au@Ag) nanostructures [48]. Briefly, 250 µL of HauCl₄·4H₂O (10 wt%) was added to 250 mL of deionized water and heated to boiling under stirring. Then, 2.5 mL of a 1 wt% sodium citrate solution was quickly added to the boiling mixture, which changed color from pale yellow to wine red. The solution was stirred for another 15 min after which heating was stopped, and stirring continued until the solution cooled to room temperature. The gold nanoparticles (Au NPs) were centrifuged at 9000 rpm for 20 min, redispersed in 250 mL of deionized water, and stored at 4 °C for later use. Next, the Ag shell was prepared by heating 250 mL of the Au NPs solution to 60 °C and adding 6 mL of a 1 wt% sodium citrate solution. The mixture was heated to boiling, and 2.5 mL of silver nitrate solution was added. After stirring for 40 min, the solution changed color from wine red to purple and finally to caramel. Stirring was continued until the solution cooled to room temperature, completing the preparation of the Au@Ag. In the second step, the synthesis of WS₂/Au@Ag was carried out. 10 mL (0.01 mg/mL) of WS₂ aqueous solution was added into 30 mL of Au@Ag colloid. The mixture

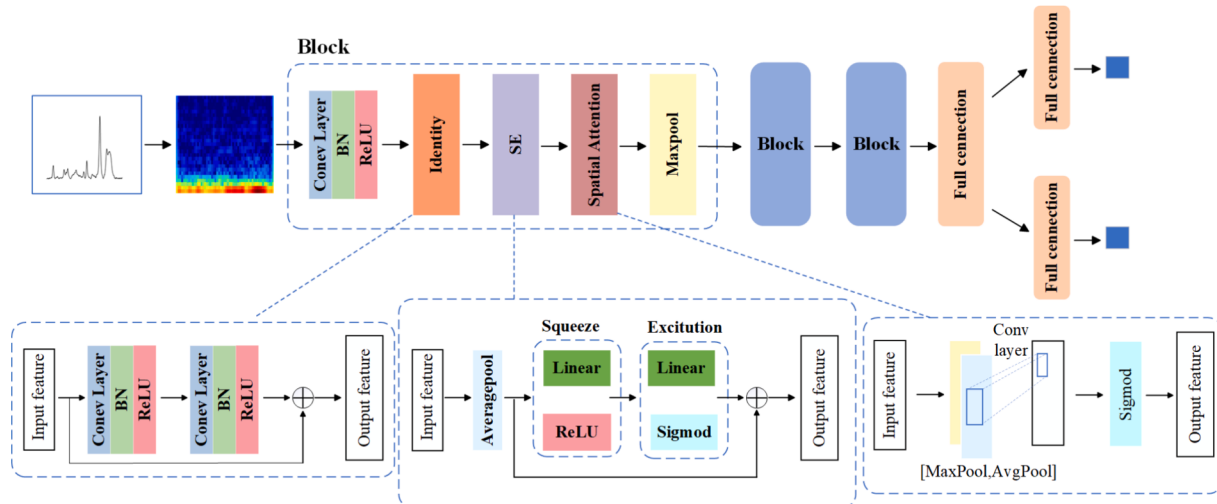


Fig. 3. Model structure of the proposed 2D-CNN.

was sonicated for 3 min and then continuously stirred for 2 h to ensure thorough mixing. The Au NPs were centrifuged at 9000 rpm for 20 min.

The hybrid substrate was characterized using ultraviolet-visible (UV–Vis) spectroscopy, particle size analysis, Raman spectroscopy, scanning electron microscopy (SEM), and transmission electron microscopy (TEM). The UV–Vis spectra of Au, Au@Ag, and WS₂/Au@Ag nanoparticles were recorded using an Evolution 350 UV–Vis spectrophotometer (Thermo Fisher Scientific, China) in the wavelength range of 200–800 nm with a spectral resolution of 1 nm, integration time of 0.3 s, and scan speed of 1200 nm/min [49]. The size distribution of WS₂/Au@Ag nanoparticles was measured by dynamic light scattering experiments (Zetasizer, Nano-ZS90, Malvern, UK). The surface morphology and size of WS₂/Au@Ag nanoparticles were characterized by JEM-2100F (JEOL, Japan) high-resolution transmission electron microscopy at an accelerating voltage of 200 kV.

2.3. Substrate performance

Using rhodamine 6G (R6G) as a Raman probe to explore the detection limit of WS₂/Au@Ag, a series of R6G concentration gradients from 10⁻¹ M to 10⁻¹⁴ M were prepared. Since the signal intensity of high concentrations of R6G exceeds the instrument's maximum limit, the detection started from 10⁻⁷ M. 3 μL of the substrate solution were dropped onto a microscope slide, then wait until the edges are slightly dry. Subsequently, 3 μL of the corresponding concentration of R6G solution were added to the substrate. Ten data points were randomly collected, and their average was taken as the Raman spectrum for that concentration. To compare the enhancement effects of the two substrates, WS₂/Au@Ag and Au@Ag, the same volume of 10⁻⁷ M R6G were dropped onto both substrates for SERS spectral analysis. Following the same procedure, 3 μL of a 10⁻⁷ M R6G solution were added to the substrate, and 100 data points were randomly collected. The Raman characteristic peaks and intensities were observed to assess uniformity.

2.4. Preparation of ceftriaxone, ampicillin and vancomycin solutions

2.4.1. Preparation of standard solutions of ceftriaxone, ampicillin and vancomycin

The preparation of standard solutions was based on a consistent protocol. Using ceftriaxone as an example, standard solutions were prepared by dissolving ceftriaxone powder in deionized water and diluting to a series of concentrations (0.5–1000 μg/mL). 3 mL of deionized water were mixed with 3 mg of ceftriaxone powder, and the mixture was ultrasonically dissolved to obtain a 1000 μg/mL ceftriaxone

standard solution. 1 mL of this 1000 μg/mL solution was diluted with 1 mL of deionized water to obtain a 500 μg/mL solution, and so forth, resulting in a series of concentration gradients: 0.5 μg/ml, 1 μg/ml, 5 μg/ml, 10 μg/ml, 50 μg/ml, 100 μg/ml, 500 μg/ml, 1000 μg/ml.

2.4.2. Preparation of ceftriaxone, ampicillin and vancomycin serum solutions

In this study, fetal bovine serum (FBS) solution was used to simulate the complex blood environment of clinical samples. Taking ceftriaxone serum solution as an example, firstly, 1 mL of fetal bovine serum was diluted in 9 mL of deionized water to form a volume concentration of 10 % fetal bovine serum. Subsequently, in the same way as the standard ceftriaxone solution, with the deionized water replaced by 10 % fetal bovine serum to obtain the corresponding concentration.

2.4.3. Preparation of mixed serum solution of ceftriaxone and ampicillin

Considering that ceftriaxone and ampicillin are often used in combination in the clinic, it would be meaningful to quantify multiple antibiotics in more complex samples [5]. *Escherichia coli* has different MIC for different antibiotics. In general, the effective antimicrobial drug concentration should be 4–8 times the MIC [18]. In this study, based on previous works and the European Committee on Antimicrobial Susceptibility Testing (EUCAST) guidelines, the MIC of ceftriaxone in the treatment of *Escherichia coli* was 2 μg/mL [50] and that of ampicillin was 4 μg/mL. We prepared seven different concentrations of antibiotics (0.5MIC, MIC, 4MIC, 6MIC, 8MIC, 12MIC, 16MIC) around their respective MIC values. In the mixed solutions, the concentrations of ceftriaxone were 0.5 μg/mL, 1 μg/mL, 4 μg/mL, 6 μg/mL, 8 μg/mL, 12 μg/mL, and 16 μg/mL, while the concentrations of ampicillin were 2 μg/mL, 4 μg/mL, 16 μg/mL, 24 μg/mL, 32 μg/mL, 48 μg/mL, and 64 μg/mL. Then, 49 different combinations of mixed antibiotics were prepared to cover the range of concentrations that were detailed in Supplementary Table S1.

2.5. SERS detection of ceftriaxone, ampicillin and vancomycin powders and solutions

All Raman and SERS spectra were acquired using a laser confocal Raman microscope (LabRAM Xplora Plus, HORIBA Scientific, France) with a spectral range of 300–1800 cm⁻¹ and a laser excitation wavelength of 638 nm, using a 10x objective lens. An integration time of 10 s was used for detecting powders, while an integration time of 5 s was used for detecting solutions. First, the Raman spectra of ceftriaxone, ampicillin, and vancomycin powders were collected, with a small

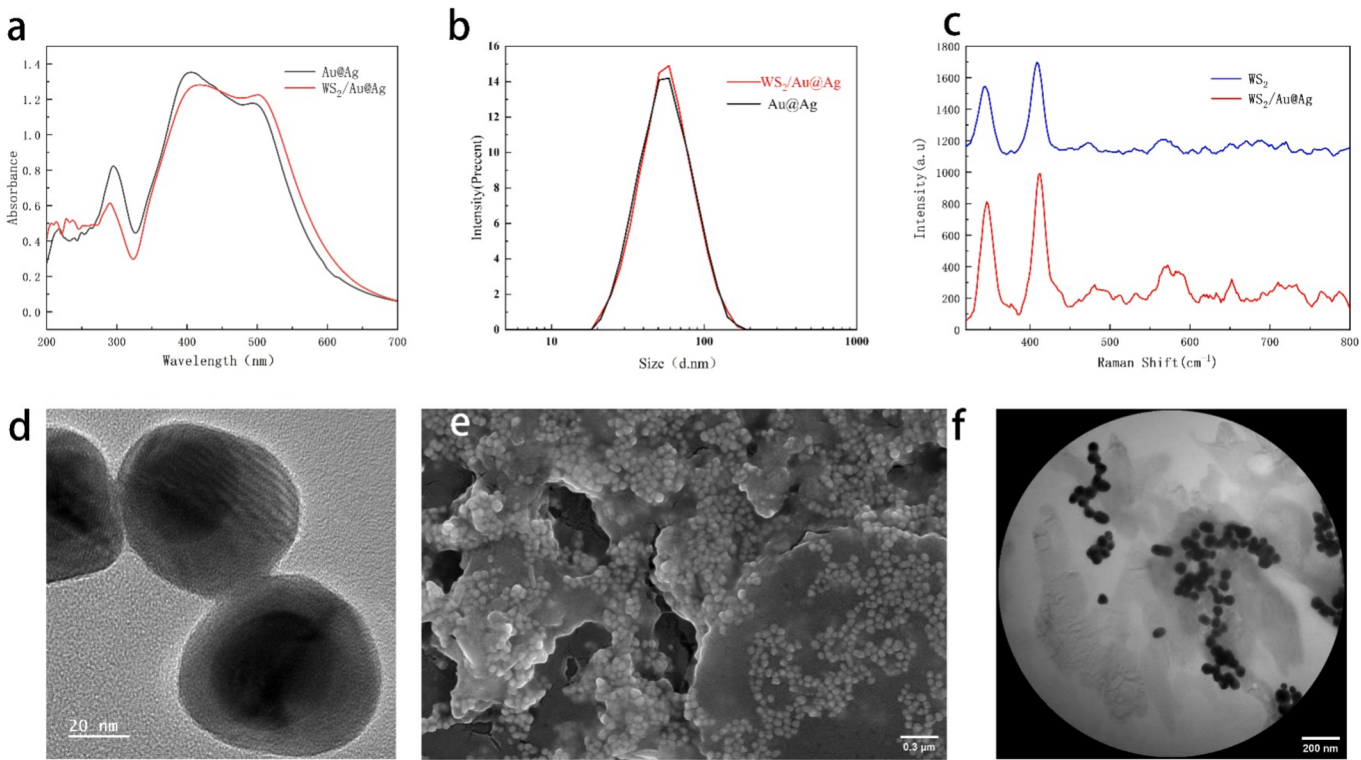


Fig. 4. (a) UV–VIS spectra of $\text{WS}_2/\text{Au}@\text{Ag}$ and $\text{Au}@\text{Ag}$; (b) particle size distribution of $\text{WS}_2/\text{Au}@\text{Ag}$ and $\text{Au}@\text{Ag}$ obtained by dynamic light scattering; (c) SERS spectra of $\text{WS}_2/\text{Au}@\text{Ag}$ and WS_2 ; (d) TEM image of $\text{Au}@\text{Ag}$; (e) SEM image of $\text{WS}_2/\text{Au}@\text{Ag}$; (f) TEM image of $\text{WS}_2/\text{Au}@\text{Ag}$.

amount of the powders directly being placed on a microscope glass slide and put under the microscope for measurement. In the second step, Raman spectra of ceftriaxone, ampicillin and vancomycin solutions were collected. Before that, to ensure that water and FBS do not interfere with the SERS detection of antibiotics, the SERS spectra of water and FBS with the $\text{WS}_2/\text{Au}@\text{Ag}$ were collected. The measurement of solution samples was performed with SERS with the $\text{WS}_2/\text{Au}@\text{Ag}$ substrate prepared in 2.2. 3 μL of $\text{WS}_2/\text{Au}@\text{Ag}$ was dropped onto a microscope slide and allowed to sit for a moment until a coffee ring formed at the edge of the substrate, while most of the area remained colloidal. Then, 3 μL of the test sample solution was dropped onto the substrate, followed by the SERS detection of the sample.

2.6. Spectral data processing and model establishment

2.6.1. Collection and preprocessing of original spectra

Raman or SERS spectra were collected with 6 repetitions for each sample. For the quantification of the analysts, the correlation between the intensity of characteristic peaks and the concentration of an analyst was established. Here, the logarithmic intensities ($\log I$) of the Raman characteristic peaks of ceftriaxone, ampicillin, and vancomycin were linearly related to the logarithmic concentrations ($\log C$) of the antibiotic samples. The log–log relationship was typically used when the measured range covered at least several orders of magnitudes [51,52]. The linearity for each analyst was evaluated using R^2 . The limit of detection (LOD) was calculated based on the definition as three times the instrument background signal value produced by matrix blanks ($S/N = 3$), as described in the literature [53].

2.6.2. 2D-CNN regression model

This study proposes a regression model based on a two-dimensional convolutional neural network (2D-CNN) to predict the concentrations of ceftriaxone and ampicillin in mixed solutions, as illustrated in Fig. 3. By subjecting SERS spectroscopy data to short-time Fourier transform

(STFT), it is converted into a format suitable for 2D-CNN processing. STFT provides the distribution of the signal in the frequency domain, revealing the frequency composition of the signal over different time segments, thereby enabling the model to identify local patterns more effectively. The architecture of the model consists of three main components: identity blocks, squeeze-and-excitation (SE) blocks, and spatial attention modules. Identity blocks adopt a residual learning framework, mapping features through two convolutional layers while introducing skip connections to maintain the integrity of input information, effectively avoiding issues of gradient vanishing or exploding. The SE block captures global information from each feature map via global average pooling and adjusts the weights of each feature channel dynamically through two fully connected layers, achieving cross-channel feature recalibration. The spatial attention module utilizes global pooling techniques to generate spatial weights, enhancing the contribution of information from critical regions while suppressing the influence of irrelevant areas. The combination of these modules enables the network to learn complex patterns within SERS spectroscopic data more efficiently. Following this, further compression of the feature maps to a size of 28×28 is achieved through subsequent pooling operations, after which a series of fully connected layers output the predicted concentrations of the drug.

2.6.3. SERS data analysis of mixed analysts using the 2D-CNN model

SERS-enhanced spectra with different forms of deviation from the original samples were often introduced to ensure robust training of the model and prevent overfitting [40]. In this study, four different enhancement methods were adopted based on the literature [40]. The details of these methods are provided in the supplementary. With data enhancement, the number of spectra for each concentration increased from 20 to 260. This resulted in a total number of 12,740 spectra, which enhanced the richness and diversity of the dataset for robust model training. Subsequently, the 12,740 SERS spectra were transformed into two-dimensional spectra using spectral short-time Fourier transform

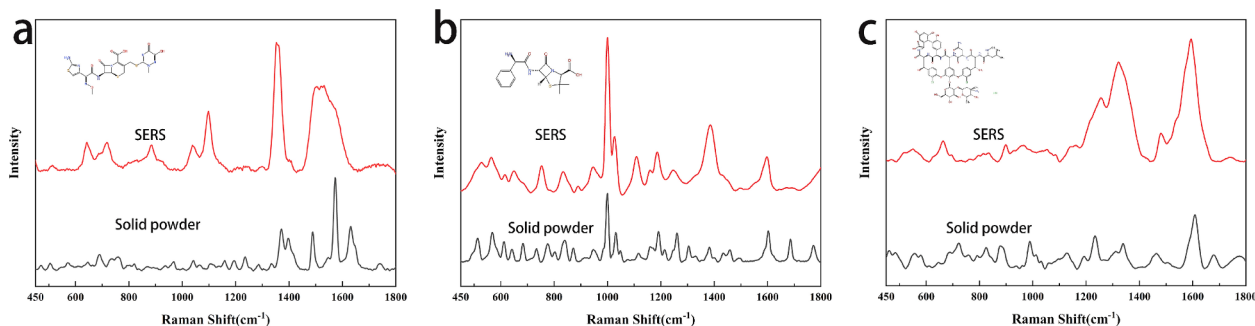


Fig. 5. Raman spectrum of powder and SERS spectrum of solution for (a) ceftriaxone (b) ampicillin (c) vancomycin.

(SSTFT), where the x-axis represents wavenumber position and the y-axis represents intensity [54]. Based on the original spectrum as well as the enhanced SERS spectrum, the dataset was divided into 8820 spectra for the training set and 3920 spectra for the testing set [40,55]. An error back-propagation algorithm along with the stochastic gradient descent optimization method, adaptive moment estimation (Adam) was used to iteratively optimize the CNN parameters to minimize the loss function. After iterating for 50 epochs, the loss function gradually decreased and eventually stabilized. In this study, (R^2) and root mean square error (RMSE) were used as two metrics to evaluate the performance of the model. The formulas are provided in the supplementary. Finally, the regression performance of the 2D-CNN was compared with that of 1D-CNN and other traditional regression methods, including Principal Component Analysis with One-Dimensional Convolutional Neural Network (PCA-1D-CNN), Random Forest Regression (RFR), Support Vector Regression (SVR) and Partial Least Squares Regression (PLSR). R^2 and RMSE were used as evaluation parameters of model performance.

3. Results and discussion

3.1. Characterization of WS₂/Au@Ag

The WS₂/Au@Ag substrate was characterized with UV-Vis spectroscopy, dynamic light scattering experiments and electron microscopy. As shown in Fig. 4a, the peaks at 415 nm and shoulder at 504 nm corresponded to the silver shells and gold cores, respectively, which were consistent with the UV-Vis absorption peaks of Ag and Au [56]. A small peak appears at around 230 nm for WS₂/Au@Ag, which is the absorption peak of WS₂, indicating the successful conjugation of WS₂ onto Au@Ag nanoparticles [57–59]. The particle size distribution of WS₂/Au@Ag and Au@Ag was obtained through dynamic light scattering. As shown in the Fig. 4b, the particle size distribution curve presents a single peak without any multi-peak phenomena. The particle size distribution chart indicates that the particle dimensions are concentrated within a very narrow range, with the particle sizes mainly centered around 50 nm, demonstrating extremely high particle size uniformity. At the same time, it can be found that since Au@Ag was adsorbed on the thin layer of WS₂, it did not change the overall particle size. Fig. 4c showed the Raman peaks of WS₂/Au@Ag and WS₂, and it can be clearly seen that there were two different peaks at 352 cm⁻¹ and 419 cm⁻¹ corresponding to the E_{2g}¹ and A_{1g} vibrational modes of WS₂ [60]. Considering the influence of WS₂ within the range from 300 cm⁻¹ to 450 cm⁻¹, the SERS wavenumber range for antibiotics was adjusted to 450 cm⁻¹ to 1800 cm⁻¹ for subsequent experiments. The TEM image of Au@Ag in Fig. 4d clearly showed the core-shell structure with an average size of approximately 50 nm. The darker region corresponds to the gold core, while the lighter outer region represents the silver shell. The SEM and TEM images of WS₂/Au@Ag revealed the crumpled layered structure of WS₂ and the uniform adsorption of Au@Ag particles on the WS₂ surface, which further indicated the excellent uniformity of the synthesized WS₂/Au@Ag substrate.

The enhancement effect of WS₂/Au@Ag and Au@Ag was compared by SERS assays performed on R6G at a concentration of 10⁻⁷ M. Taking the peak at 1509 cm⁻¹ as an example, the signal intensity of WS₂/Au@Ag was approximately 1.7 times that of Au@Ag. It can be seen from this that the enhancement effect of this composite substrate, which combined a two-dimensional material with a noble metal, was superior to that of a single noble metal substrate. Subsequently, R6G was used as a Raman probe to further investigate the detection limit of this composite substrate. The detection limit for R6G can be as low as 10⁻¹⁴ M, once again demonstrating the excellent enhancement effect of this substrate. 100 random locations of SERS assays were performed on 10⁻⁷ M of R6G to examine the SERS reproducibility of WS₂/Au@Ag. For more details, please refer to Fig. S1. To quantitatively evaluate the enhancement effect of SERS, Le et al. proposed the concept of the Analytical Enhancement Factor (AEF), whose definition is provided in the supplemental document. According to the formula, we calculated the enhancement factor of the substrate to be 2.98 × 10⁶.

3.2. Raman and SERS spectral assignments of ceftriaxone, ampicillin and vancomycin

The SERS spectrum of 1000 µg/mL standard solution samples of antibiotics were obtained using the WS₂/Au@Ag substrate and compared with the Raman spectrum of powder samples, as shown in Fig. 5.

By comparing the SERS spectrum of the three antibiotic powders and their corresponding SERS spectrum, it was observed that the characteristic peak positions were mostly similar, despite some minor shifts which may be attributed to the binding of the substrate to the analyte molecules and the change of the environment around the molecules. The specific peak positions and their assignments were listed in Supplementary Table S2, the major Raman characteristic peaks obtained experimentally were also consistent with previously reported Raman peaks of ceftriaxone, ampicillin and vancomycin. In this study, in order to quantify the three antibiotics, we took 1353 cm⁻¹ (carboxylate group), 1000 cm⁻¹ (benzene ring vibration) and 1594 cm⁻¹ (amide I carboxyl group (C = O)) to represent ceftriaxone [14,61] ampicillin [62,63] and vancomycin [64] (C = O), respectively.

3.3. SERS assay of single and mixed antibiotic solutions

3.3.1. Single standard solutions

SERS spectra of water and FBS demonstrated that water and FBS as solvents do not affect the accuracy of antibiotic detection, as shown in Fig. S2. SERS detection was performed on standard solutions of the three antibiotics at eight different concentrations as shown in Fig. 6, which encompasses the clinically required concentration range. Based on the SERS intensities at specific characteristic peaks, a quantitative study was conducted for three antibiotics. Due to the presence of large “hot spots” between WS₂/Au@Ag nanoparticles, the SERS signals were enhanced to varying degrees with increasing antibiotic concentration. We can

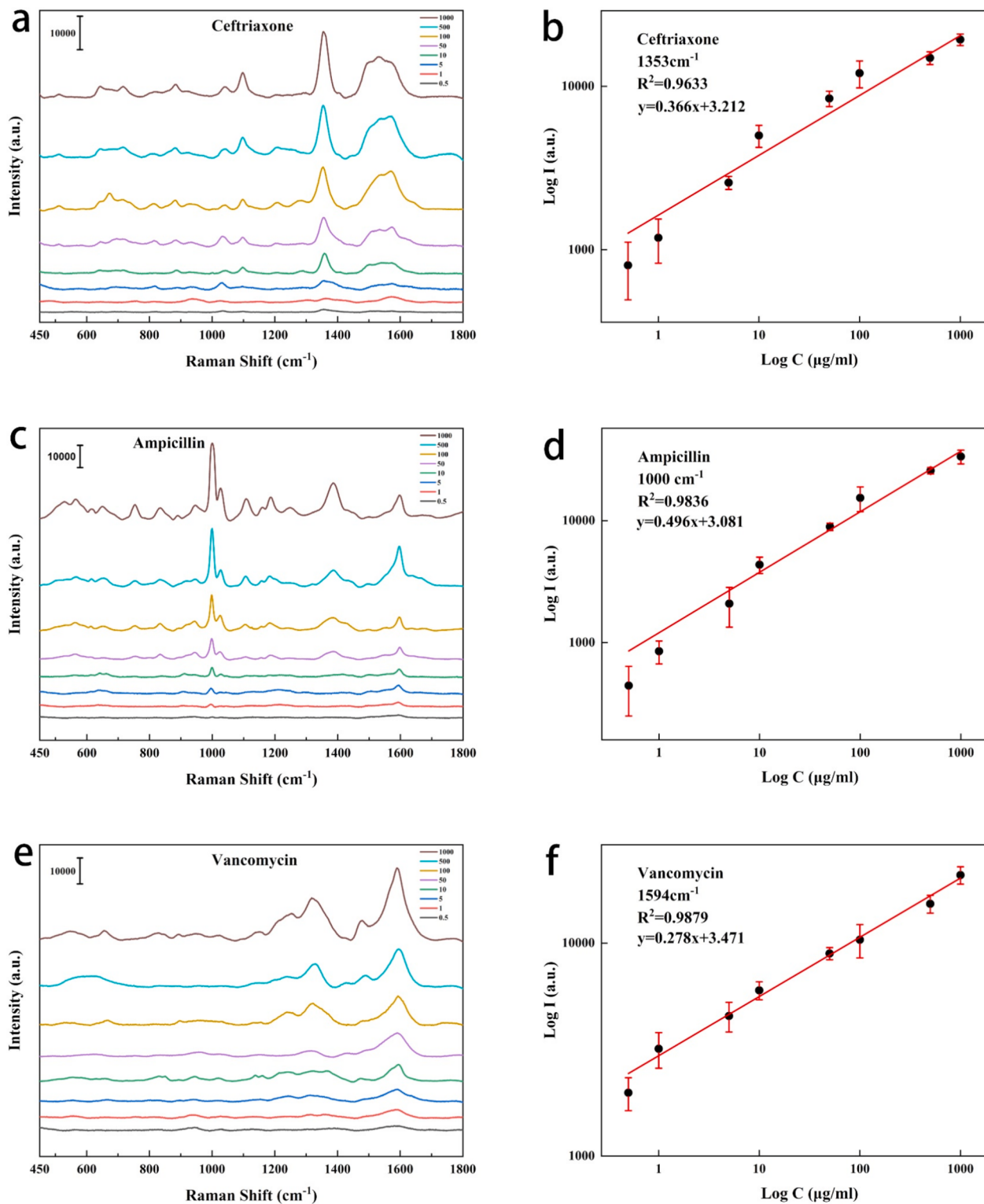


Fig. 6. SERS spectra and linear regression results of ceftriaxone (a, b) ampicillin (c, d) and vancomycin (e, f) standard solutions. Concentration unit: µg/mL.

observe that even at the lowest concentration of 0.5 µg/ml, the characteristic peaks representing the three antibiotics can be observed. The logarithms of the concentrations at 1353 cm⁻¹, 1000 cm⁻¹, and 1594 cm⁻¹ showed good correlations with the logarithms of the SERS intensities, with R^2 values of 0.96332, 0.98355, and 0.9878, respectively.

3.3.2. Single serum solutions

In practical clinical applications, TDM of the antibiotics is usually

performed with blood samples. Here, 10 % fetal bovine serum was used to simulate the complex serum environment of the human body. SERS detection was performed on serum solutions of the three antibiotics at eight different concentrations as shown in Fig. 7.

The SERS spectrum peak positions of the serum samples were very similar to those of the standard solutions, with satisfactory linear fits at 1353 cm⁻¹, 1000 cm⁻¹, and 1594 cm⁻¹, respectively. However, compared to the SERS spectrum of the standard solutions, the

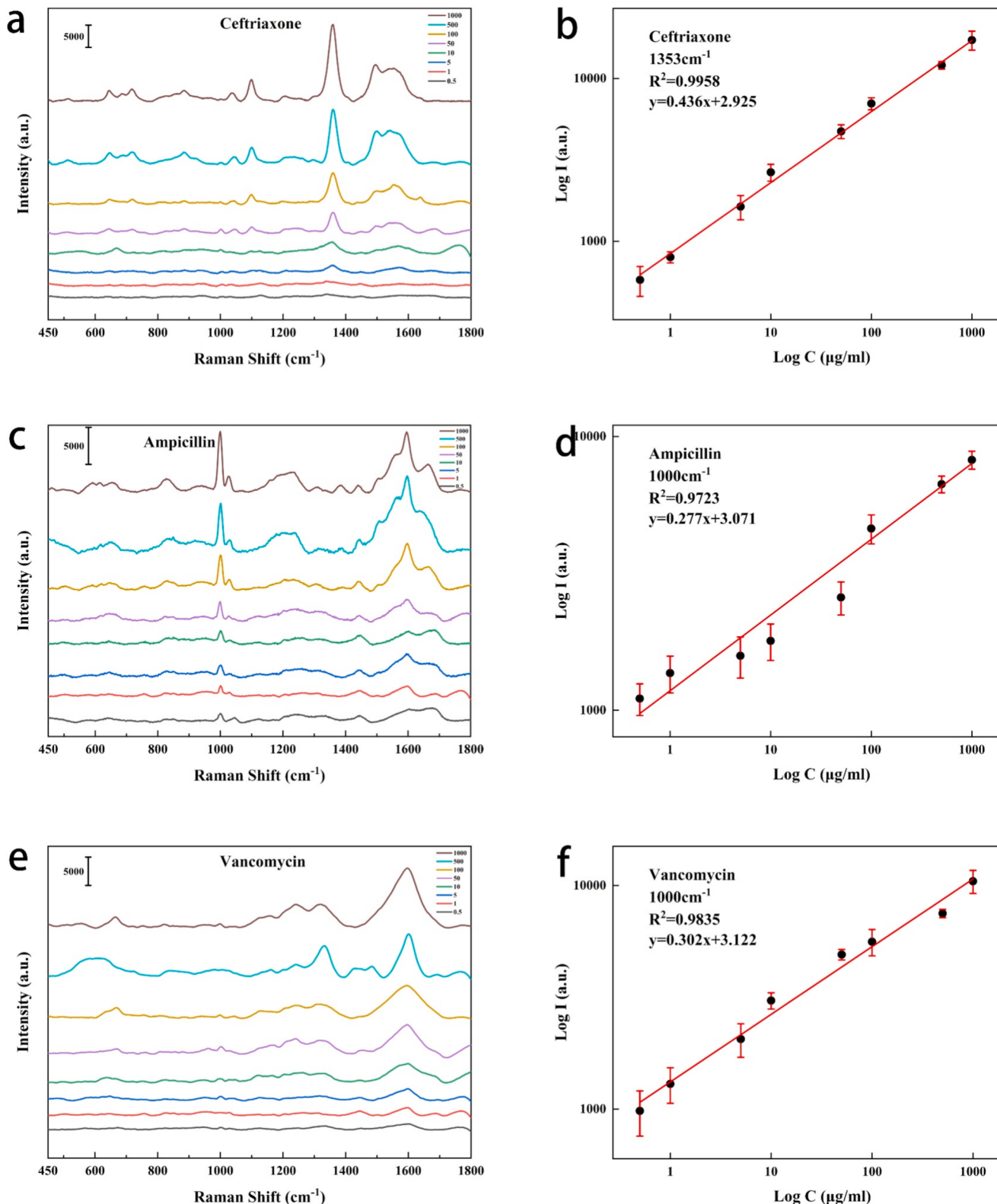


Fig. 7. SERS spectra and linear regression results of ceftriaxone (a, b) ampicillin (c, d) and vancomycin (e, f) serum solutions. Concentration unit: $\mu\text{g}/\text{mL}$.

characteristic peak intensities in the serum solutions were moderately lower at the same concentration (Fig. S3). This was possibly due to the interference of various plasma proteins, peptides, fats, carbohydrates, growth factors, hormones, inorganic substances, etc., which occupy part of the hot spots on the substrate and reduce the density of hot spots available for target molecules [65]. At the characteristic peak of

ceftriaxone at 1353 cm^{-1} , the SERS spectrum intensity showed an excellent linear relationship with the ceftriaxone concentration in the range of $0.5 \mu\text{g}/\text{mL}$ to $1000 \mu\text{g}/\text{mL}$. Similar regression results were observed for the characteristic peaks of ampicillin serum samples and vancomycin serum samples within the entire detection range. The R^2 values were 0.96332, 0.98355, and 0.98786, respectively. According to

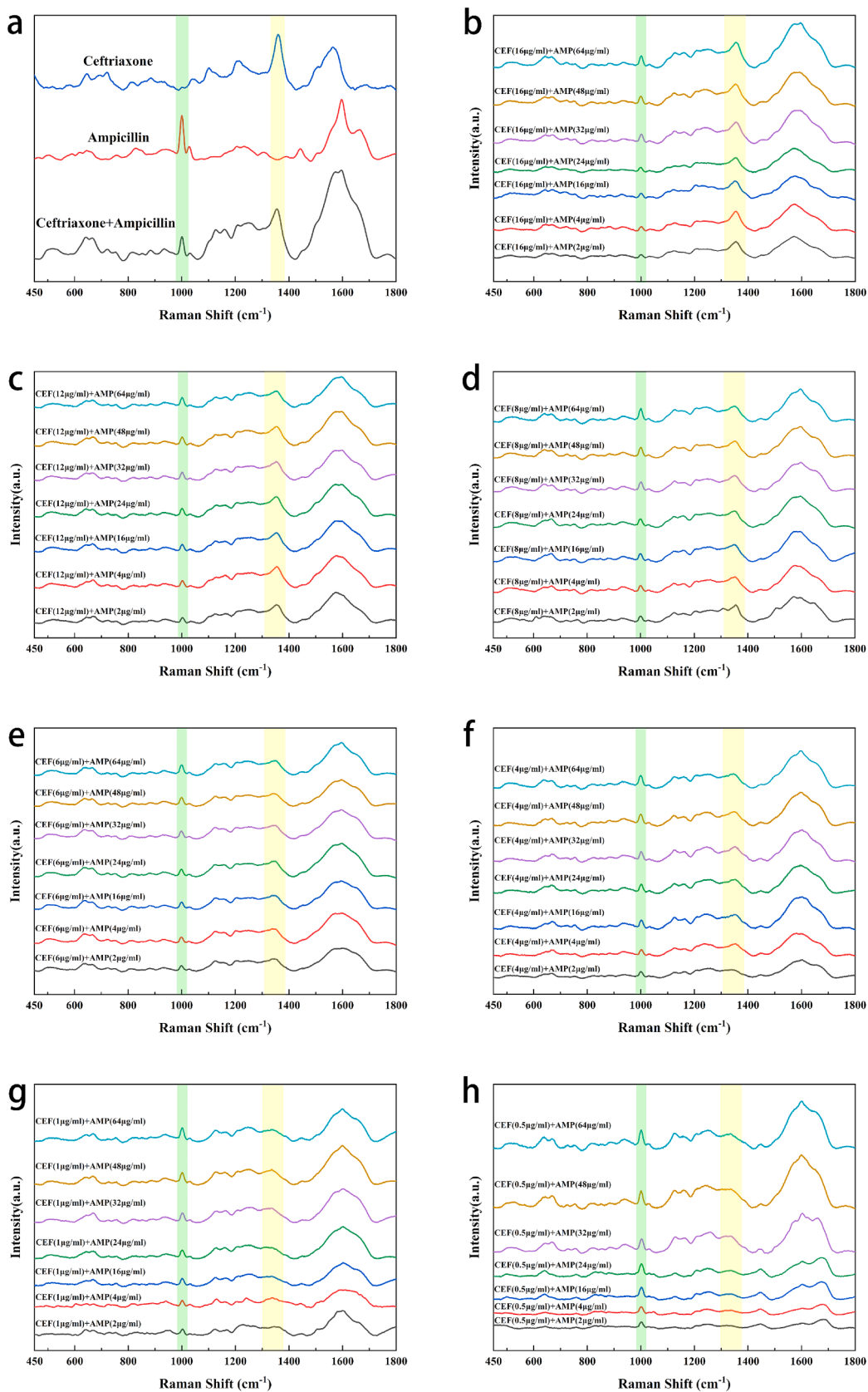


Fig. 8. (a) SERS spectra of ceftriaxone, ampicillin, and mixed solutions; (b)–(h) SERS spectra of 49 groups of mixed solutions with static ceftriaxone concentrations.

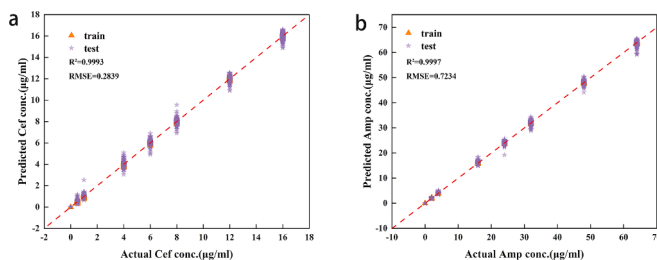


Fig. 9. Antibiotic prediction performance for ceftriaxone (a) and ampicillin (b) using 2D-CNN.

Table 1
Regression performance of different models.

	2D-CNN	1D-CNN	PCA-1D-CNN	RFR	SVR	PLSR
R^2	0.9993	0.9837	0.9850	0.89	0.94	0.57
R^2_a	0.9997	0.9809	0.9817	0.83	0.69	0.71
$RMSE_c$	0.2839	1.3458	1.2912	3.51	2.61	13.23
$RMSE_a$	0.7234	5.8276	5.0983	17.48	23.53	22.68

the LOD formula, the LODs were calculated to be 0.266 $\mu\text{g/mL}$ for ceftriaxone, 0.3191 $\mu\text{g/mL}$ for ampicillin, and 0.1402 $\mu\text{g/mL}$ for vancomycin. Therefore, we can use this method to perform qualitative and quantitative analyses of antibiotics in real samples, providing data support for clinical drug guidance.

3.3.3. Mixed serum solutions

In the clinical treatment of neonatal sepsis, ceftriaxone and ampicillin are often used in combination to control the progression of the disease. Considering the practical application scenarios, SERS detection on mixed solutions of ceftriaxone and ampicillin was performed (Fig. 8). It can be seen that in the mixed solution, all the representative SERS peaks of ceftriaxone and ampicillin were present, with yellow highlight representing the 1354 cm^{-1} characteristic peak of ceftriaxone and green highlight representing the 1000 cm^{-1} characteristic peak of ampicillin. This indicated that the simultaneous qualitative detection of ceftriaxone and ampicillin in mixed solutions was feasible. Seven different concentrations of antibiotics were prepared around their MICs, simulating low, effective and excessive antibiotic concentration scenarios. Mixing the seven concentrations of the two antibiotics resulted in 49 mixed solutions, and SERS spectral detection was performed on these 49 mixed solution groups, with 20 independent measurements collected for each concentration. For better visualization, Fig. 8b to h displayed constant ceftriaxone concentration and gradually increasing ampicillin concentrations. In each figure, the constant ceftriaxone concentration presented stable signal intensity at 1354 cm^{-1} , while the different concentrations of ampicillin show intensity gradients, which can be observed at 1354 cm^{-1} . This trend demonstrated the potential of quantifying each drug in the mixed solutions. However, the quantification of multiple chemicals in one sample was more difficult because they no longer follow linear relationships.

3.4. Prediction of antibiotic concentration in mixed solutions with the 2D-CNN model

Combining CNN with quantitative analysis of SERS spectra brings great prospects for the promotion of SERS technology in TDM. In this paper, 2D-CNN quantitative analysis model was constructed to predict the corresponding antibiotic concentration by analyzing the different intensities of antibiotic characteristic peaks at different concentrations. The model showed good performance in concentration regression, and the final results for ceftriaxone and ampicillin are shown in Fig. 9a and b. The results are summarized as follows. The R^2 of ceftriaxone and ampicillin in the test set were 0.9993 and 0.9997, and the RMSE was

0.2839 $\mu\text{g/mL}$ and 0.7234 $\mu\text{g/mL}$, respectively. The high R^2 and lower RMSE demonstrated that the 2D-CNN model had an excellent capability for quantitative analysis. The regression performance of 2D-CNN, 1D-CNN and other conventional regression methods such as PCA-1D-CNN, RFR, SVR and PLSR (Table 1) were also compared.

Ampicillin has a smaller range of variation in the intensity of its characteristic peaks with changes in concentration, which adds difficulty in accurately predicting its concentration values. As a result, its RMSE was higher compared to that of ceftriaxone. This trend was consistent across all models. Through comparison, we found that CNN significantly outperformed traditional machine learning techniques in terms of both R^2 and RMSE. Both CNN models achieved an R^2 over 0.98, with RMSE values below 10 for each. The performance of RFR, SVR and PLSR was less satisfactory, with R^2 values of 0.89, 0.94 and 0.57, and R^2_a values of 0.83, 0.69 and 0.71, respectively. This was due to CNN's strong learning capabilities, which can automatically extract key features from input spectrum. Traditional machine learning models had insufficient capability to extract features and lack the ability to learn complex patterns, resulting in lower evaluation metrics. The PCA-1D-CNN model slightly outperformed 1D-CNN due to its feature extraction, yet it was still inferior when compared to 2D-CNN. Based on Table 1, it was found that 2D images serve as a better input choice compared to 1D data. 2D images not only include the wavenumber position information and intensity information of the spectrum itself but also contain artificially created spatial features. The information in the 2D images allowed for increased propagation and nonlinearity, leading to more accurate predictions of antibiotic concentrations in mixed solutions.

4. Conclusion

In this paper, an effective protocol for the label-free and highly sensitive detection of ceftriaxone, ampicillin and vancomycin in serum using $\text{WS}_2/\text{Au@Ag}$ core-shell nanostructures was presented. The $\text{WS}_2/\text{Au@Ag}$ substrate was demonstrated to have superior enhancement effect, with the detection limit of R6G being 10^{-14} M . For the determination of antibiotics, this method can determine ceftriaxone, ampicillin and vancomycin qualitatively and quantitatively at an extremely low concentration of 0.5 $\mu\text{g/mL}$ with a linear range of 0.5–1000 $\mu\text{g/mL}$, respectively. The detection limits of the three antibiotics were 0.266 $\mu\text{g/mL}$, 0.3191 $\mu\text{g/mL}$ and 0.1402 $\mu\text{g/mL}$, covering the clinically required TDM ranges. We have also developed a regression model for the concentration prediction of multiple antibiotics simultaneously using SERS and a 2D-CNN deep learning algorithm. For mixed ceftriaxone and ampicillin solutions, the 2D-CNN regression model processed the complex spectra to predict the individual concentrations of the two antibiotics accurately, reaching an R^2 value of over 0.99 for both antibiotics, with RMSE values of 0.2839 $\mu\text{g/mL}$ and 0.7234 $\mu\text{g/mL}$, respectively. The combination of deep learning with SERS detection offers a significant leap forward in the analysis of complex SERS spectra and provides a solution for TDM-based antibiotic prediction in neonatal sepsis, bringing great promises to personalized medicine.

Funding

This work was supported by the National Natural Science Foundation of China (NSFC) (No. 62275156).

Declaration of competing interest

The authors declare that they have no known competing financial interests or personal relationships that could have appeared to influence the work reported in this paper.

Appendix A. Supplementary data

Supplementary data to this article can be found online at <https://doi.org/10.1016/j.saa.2025.125850>.

Data availability

Data underlying the results presented in this paper are not publicly available at this time but may be obtained from the authors upon reasonable request.

References

- [1] C. Fleischmann-Struzek, D.M. Goldfarb, P. Schlattmann, L.J. Schlapbach, K. Reinhart, N. Kissoon, The global burden of paediatric and neonatal sepsis: a systematic review, *Lancet Respiratory Med.* 6 (2018) 223–230.
- [2] 侯齐书, 叶继峰, 杨莲华, 早发型与晚发型新生儿败血症临床特点及病原学比较, *中国消毒学杂志* 34 (2017) 4.
- [3] E. Sharland, S. Qazi, P. Heath, M. Balasegaram, J. Bielicki, M. Sharland, Can the history of empiric antibiotic treatment for neonatal sepsis inform future global trials? *Clin. Microbiol. Infect.* 28 (2022) 1313–1315.
- [4] J. van den Anker, K. Allegaert, Rational use of antibiotics in neonates: still in search of tailored tools, *Healthcare* 7 (2019).
- [5] t. S. o. P. C. M. A. Subspecialty Group of Neonatology, and N. S. C. M. D. A. Professional Committee of Infectious Diseases, Expert consensus on the diagnosis and management of neonatal sepsis (version 2019), *Zhonghua er ke za zhi = Chinese J. Pediatrics* 57 (2019) 252–257.
- [6] D. Astapenko, V. Cerny, Surviving sepsis campaign: international guidelines for management of sepsis and septic shock: 2021, *Anesteziolice a Intenzivni Medicina* 32 (2021) 249–255.
- [7] F. de Velde, J.W. Mouton, B.C.M. de Winter, T. van Gelder, B.C.P. Koch, Clinical applications of population pharmacokinetic models of antibiotics: Challenges and perspectives, *Pharmacol. Res.* 134 (2018) 280–288.
- [8] M.H. Abdul-Aziz, J.W.C. Alffenaar, M. Bassetti, H. Bracht, G. Dimopoulos, D. Marriott, M.N. Neely, J.A. Paiva, F. Pea, F. Sjovall, J.F. Timsit, A.A. Udy, S. G. Wicha, M. Zeitlinger, J.J. De Waele, J.A. Roberts, Escmid, Escmid, Isac, Antimicrobial therapeutic drug monitoring in critically ill adult patients: a Position Paper, *Intensive Care Med.* 46 (2020) 1127–1153.
- [9] E.F. Barreto, A.J. Webb, G.M. Pais, A.D. Rule, P.J. Jannetto, M.H. Scheetz, Setting the beta-lactam therapeutic range for critically ill patients: is there a floor or even a ceiling? *Crit. Care Explor.* 3 (2021) e0446.
- [10] C. Roger, B. Louart, Beta-lactam toxicity in the intensive care unit: an underestimated collateral damage? *Microorganisms* 9 (2021) 1505.
- [11] 陈桂兰, 游金兵, 张雷, 汤琼瑶, 陈作武, 万古霉素治疗新生儿败血症的血药浓度监测与疗效, *中华医院感染学杂志* 32 (2022) 5.
- [12] A. Cafaro, M. Stella, A. Mesini, E. Castagnola, G. Cangemi, F. Mattioli, G. Baiardi, Dose optimization and target attainment of vancomycin in children, *Clin. Biochem.* 125 (2024).
- [13] S.G. Wicha, A.G. Märtsönen, E.I. Nielsen, B.C.P. Koch, L.E. Friberg, J.W. Alffenaar, I. K. Minichmayr, A. Int Soc, P.P.S. Grp, From therapeutic drug monitoring to model-informed precision dosing for antibiotic, *Clin. Pharmacol. Ther.* 109 (2021) 928–941.
- [14] C. Liu, C. Franceschini, S. Weber, T. Dib, P.T. Liu, L. Wu, E. Farnesi, W.S. Zhang, V. Sivakov, P.B. Lappa, J. Popp, D. Cialla-May, SERS-based detection of the antibiotic ceftiraxone in spiked fresh plasma and microdialysis matrix by using silver-functionalized silicon nanowire substrates, *Talanta* 271 (2024).
- [15] A. Jaworska, S. Fornasaro, V. Sergio, A. Bonifacio, Potential of surface enhanced Raman spectroscopy (SERS) in Therapeutic Drug Monitoring (TDM). A critical review, *Biosensors* 6 (2016).
- [16] H.C. Ates, J.A. Roberts, J. Lipman, A.E.G. Cass, G.A. Urban, C. Dincer, On-site therapeutic drug monitoring, *Trends Biotechnol.* 38 (2020) 1262–1277.
- [17] S. Fornasaro, D. Cialla-May, V. Sergio, A. Bonifacio, The role of surface enhanced Raman scattering for therapeutic drug monitoring of antimicrobial agents, *Chemosensors* 10 (2022).
- [18] S. Dhaese, S. Van Vooren, J. Boelens, J. De Waele, Therapeutic drug monitoring of β-lactam antibiotics in the ICU, *Expert Rev. Anti Infect. Ther.* 18 (2020) 1155–1164.
- [19] J.T. Zheng, J.Y. Liu, Y.J. Zhuo, R.H. Li, X. Jin, Y. Yang, Z.B. Chen, J. Shi, Z.Y. Xiao, W.J. Hong, Z.Q. Tian, Electrical and SERS detection of disulfide-mediated dimerization in single-molecule benzene-1,4-dithiol junctions, *Chem. Sci.* 9 (2018) 5033–5038.
- [20] Y.D. Sun, P. Peng, R.Y. Guo, H.H. Wang, T. Li, Exonuclease III-boosted cascade reactions for ultrasensitive SERS detection of nucleic acids, *Biosens. Bioelectron.* 104 (2018) 32–38.
- [21] F.Q. Huang, G.S. Ma, J.Z. Liu, J. Lin, X. Wang, L. Guo, High-yield synthesis of hollow octahedral silver nanocages with controllable pack density and their high-performance sers application, *Small* 12 (2016) 5442–5448.
- [22] L.Y. Wang, P. Ma, H. Chen, M. Chang, P. Lu, N. Chen, X.D. Zhang, Y.H. Li, M.X. Sui, Rapid and ultrasensitive detection of acute kidney injury biomarkers CH3L1 and L-FABP using surface-enhanced Raman spectroscopy, *Spectrochim. Acta Part A-Mol. Biomol. Spectroscopy* 295 (2023).
- [23] C. Liu, S. Weber, R. Peng, L. Wu, W.S. Zhang, P.B. Lappa, J. Popp, D. Cialla-May, Toward SERS-based therapeutic drug monitoring in clinical settings: Recent developments and trends, *Trac-Trends Anal. Chem.* 164 (2023).
- [24] M. Pannico, P. Musto, SERS spectroscopy for the therapeutic drug monitoring of the anticancer drug 6-Mercaptopurine: Molecular and kinetic studies, *Appl. Surf. Sci.* 539 (2021).
- [25] X. Jiang, J. Zhang, L. Xu, W.E. Wang, J. Du, M.H. Qu, X.X. Han, L.B. Yang, B. Zhao, Ultrasensitive SERS detection of antitumor drug methotrexate based on modified Ag substrate, *Spectrochim. Acta Part A-Mol. Biomol. Spectroscopy* 240 (2020).
- [26] M. Pannico, P. Musto, pH activated colloidal nanospheres: a viable sensing platform for the therapeutic drug monitoring of the anticancer drug 6-mercaptopurine, *Appl. Surf. Sci.* 570 (2021).
- [27] Y.L. Xing, H. Fuss, J. Lademann, M.D. Huang, H. Becker-Ross, S. Florek, A. Patzelt, M.C. Meinke, S. Jung, N. Esser, A new concept of efficient therapeutic drug monitoring using the high-resolution continuum source absorption spectrometry and surface enhanced Raman spectroscopy, *Spectrochim. Acta Part B-Atomic Spectroscopy* 142 (2018) 91–96.
- [28] I.J. Hidi, M. Jahn, K. Weber, T. Bocklitz, M.W. Pletz, D. Cialla-May, J. Popp, Lab-on-a-chip-surface enhanced Raman scattering combined with the standard addition method: toward the quantification of nitroxoline in spiked human urine samples, *Anal. Chem.* 88 (2016) 9173–9180.
- [29] K.S. McKeating, M. Couture, M.P. Dinel, S. Garneau-Tsodikova, J.F. Masson, High throughput LSPR and SERS analysis of aminoglycoside antibiotics, *Analyst* 141 (2016) 5120–5126.
- [30] S. Muneer, D.K. Sarfo, G.A. Ayoko, N. Islam, E.L. Izake, Gold-deposited nickel foam as recyclable plasmonic sensor for therapeutic drug monitoring in blood by surface-enhanced Raman spectroscopy, *Nanomaterials* 10 (2020).
- [31] B. Zhao, D.Y. Shen, Z.C. Zhang, P. Lu, M. Hossain, J. Li, B. Li, X.D. Duan, 2D metallic transition-metal dichalcogenides: structures, synthesis, properties, and applications, *Adv. Funct. Mater.* 31 (2021).
- [32] J. Li, T.R. Yang, J.H. Lang, H.L. Liu, M. Gao, Functionalized MoS₂: circular economy SERS substrate for label-free detection of bilirubin in clinical diagnosis, *Microchim. Acta* 190 (2023).
- [33] H. Li, Q. Zhang, C.C.R. Yap, B.K. Tay, T.H.T. Edwin, A. Olivier, D. Baillargeat, From bulk to monolayer MoS₂: evolution of Raman scattering, *Adv. Funct. Mater.* 22 (2012) 1385–1390.
- [34] S.Y. Chen, M.H. Ge, S.R. Weng, J.X. Li, Y.H. Huang, P. Li, L.B. Yang, Development of a MoS₂-Ag NP nanopocket to trap target molecules for surface-enhanced raman scattering detection with long-term stability and high sensitivity, *Anal. Chem.* 95 (2023) 10257–10264.
- [35] Z.J. Li, L. Zhai, Q.H. Zhang, W. Zhai, P. Li, B. Chen, C.S. Chen, Y. Yao, Y.Y. Ge, H. Yang, P.Z. Qiao, J.N. Kang, Z.Y. Shi, A. Zhang, H.Y. Wang, J.Z. Liang, J.W. Liu, Z.Q. Guan, L.W. Liao, V.A. Neacsu, C. Ma, Y. Chen, Y. Zhu, C.S. Lee, L. Ma, Y.H. Du, L. Gu, J.F. Li, Z.Q. Tian, F. Ding, H. Zhang, 1T'-transition metal dichalcogenide monolayers stabilized on 4H-Au nanowires for ultrasensitive SERS detection, *Nat. Mater.* (2024).
- [36] N.E. Markina, A. Markin, Determination of multiple analytes in urine using label-free SERS coupled with simple sample pretreatments, *Anal. Chim. Acta* 1332 (2024).
- [37] Y. Zhao, Y.J. Xu, X.H. Jing, W. Ma, SERS-active plasmonic metal NP-CsPbX3 films for multiple veterinary drug residues detection, *Food Chem.* 412 (2023).
- [38] G. Soufi, E. Dumont, Y. Goksel, R. Slipets, R.A. Raja, K. Schmiegelow, H. Bagheri, A. Boisen, K. Zor, Discrimination and quantification of methotrexate in the presence of its metabolites in patient serum using SERS mapping, assisted by multivariate spectral data analysis, *Biosens. Bioelectron.* X 14 (2023).
- [39] Y.Y. Jin, C. Li, Z.W. Huang, L. Jiang, Simultaneous quantitative determination of low-concentration preservatives and heavy metals in tricholoma matsutakes based on SERS and FLU spectral data fusion, *Foods* 12 (2023).
- [40] J.J. Zhu, X. Jiang, Y.W. Rong, W.Y. Wei, S.D. Wu, T.H. Jiao, Q.S. Chen, Label-free detection of trace level zearalenone in corn oil by surface-enhanced Raman spectroscopy (SERS) coupled with deep learning models, *Food Chem.* 414 (2023).
- [41] Q. Yuan, L.-F. Yao, J.-W. Tang, Z.-W. Ma, J.-Y. Mou, X.-R. Wen, M. Usman, X. Wu, and L. Wang, Rapid discrimination and ratio quantification of mixed antibiotics in aqueous solution through integrative analysis of SERS spectra via CNN combined with NN-EN model, *J. Adv. Res.* (2024).
- [42] M.G. Yang, J.J. Wang, S.Y. Quan, Q.Q. Xu, High-precision bladder cancer diagnosis method: 2D Raman spectrum figures based on maintenance technology combined with automatic weighted feature fusion network, *Anal. Chim. Acta* 1282 (2023).
- [43] Y.F. Qi, L. Yang, B.X. Liu, L. Liu, Y.H. Liu, Q.F. Zheng, D.M. Liu, J.B. Luo, Highly accurate diagnosis of lung adenocarcinoma and squamous cell carcinoma tissues by deep learning, *Spectrochim. Acta Part A-Mol. Biomol. Spectroscopy* 265 (2022).
- [44] Y.F. Qi, G.C. Zhang, L. Yang, B.X. Liu, H. Zeng, Q. Xue, D.M. Liu, Q.F. Zheng, Y. H. Liu, High-precision intelligent cancer diagnosis method: 2D Raman figures combined with deep learning, *Anal. Chem.* 94 (2022) 6491–6501.
- [45] N. Cheng, Y. Gao, S.W. Ju, X.W. Kong, J.G. Lyu, L.J. Hou, L.H. Jin, B.J. Shen, Serum analysis based on SERS combined with 2D convolutional neural network and Gramian angular field for breast cancer screening, *Spectrochim. Acta Part A-Mol. Biomol. Spectroscopy* 312 (2024).
- [46] Y.Q. Cao, W. Yang, H. Li, H. Zhang, M.Z. Li, Development of a vehicle-mounted soil organic matter detection system based on near-infrared spectroscopy and image information fusion, *Meas. Sci. Technol.* 35 (2024).
- [47] H. Jiang, J.H. Deng, C.Y. Zhu, Quantitative analysis of aflatoxin B1 in moldy peanuts based on near-infrared spectra with two-dimensional convolutional neural network, *Infrared Phys. Technol.* 131 (2023).
- [48] G. Frens, Controlled nucleation for the regulation of the particle size in monodisperse gold suspensions, *Nature (Phys. Sci.) (UK)* 241 (1973) 20–22.

- [49] G. Park, C. Lee, D. Seo, H. Song, Full-color tuning of surface plasmon resonance by compositional variation of Au@Ag core-shell nanocubes with sulfides, *Langmuir* 28 (2012) 9003–9009.
- [50] G. Wong, F. Taccone, P. Villois, M.H. Scheetz, N.J. Rhodes, S. Briscoe, B. McWhinney, M. Nunez-Nunez, J. Ungerer, J. Lipman, J.A. Roberts, β -Lactam pharmacodynamics in Gram-negative bloodstream infections in the critically ill, *J. Antimicrob. Chemother.* 75 (2020) 429–433.
- [51] X.Y. Zhu, A linear validation method of analytical procedures based on the double logarithm function linear fitting, *Anal. Chim. Acta* 1310 (2024).
- [52] T. Singtoroj, J. Tarning, A. Annerberg, M. Ashton, Y. Bergqvist, N.J. White, N. Lindegardh, N.P.J. Day, A new approach to evaluate regression models during validation of bioanalytical assays, *J. Pharm. Biomed. Anal.* 41 (2006) 219–227.
- [53] G.L. Long, J.D. Winefordner, Limit of detection. A closer look at the IUPAC definition, *Anal. Chem.* 55 (1983) 712A–A724.
- [54] M. Chang, C. He, Y. Du, Y.M. Qiu, L.Y. Wang, H. Chen, RaT: Raman Transformer for highly accurate melanoma detection with critical features visualization, *Spectrochim. Acta Part A-Mol. Biomol. Spectroscopy* 305 (2024).
- [55] Z.Y. Zhang, H.F. Li, L.L. Huang, H.J. Wang, H.J. Niu, Z.S. Yang, M.H. Wang, Rapid identification and quantitative analysis of malachite green in fish via SERS and 1D convolutional neural network, *Spectrochim. Acta Part A-Mol. Biomol. Spectroscopy* 320 (2024).
- [56] Y. Zhou, G. Zhao, J. Bian, X. Tian, X. Cheng, H. Wang, H. Chen, Multiplexed SERS barcodes for anti-counterfeiting, *ACS Appl. Mater. Interfaces* 12 (2020) 28532–28538.
- [57] W.J. Zhao, Z. Ghorannevis, L.Q. Chu, M.I. Toh, C. Kloc, P.H. Tan, G. Eda, Evolution of electronic structure in atomically thin sheets of WS₂ and WSe₂, *ACS Nano* 7 (2013) 791–797.
- [58] L.H. Zeng, L.L. Tao, C.Y. Tang, B. Zhou, H. Long, Y. Chai, S.P. Lau, Y.H. Tsang, High-responsivity UV-Vis photodetector based on transferable WS₂ film deposited by magnetron sputtering, *Sci. Rep.* 6 (2016).
- [59] M. Alamri, M.G. Gong, B. Cook, R. Goul, J.Z. Wu, Plasmonic WS₂ nanodiscs/graphene van der waals heterostructure photodetectors, *ACS Appl. Mater. Interfaces* 11 (2019) 33390–33398.
- [60] J. Zhao, Z.C. Zhang, S.S. Yang, H.L. Zheng, Y.B. Li, Facile synthesis of MoS₂ nanosheet-silver nanoparticles composite for surface enhanced Raman scattering and electrochemical activity, *J. Alloy. Compd.* 559 (2013) 87–91.
- [61] Y.L. Wong, W.C.M. Kang, M. Reyes, J.W.P. Teo, J.C.Y. Kah, Rapid detection of carbapenemase-producing enterobacteriaceae based on surface-enhanced Raman spectroscopy with gold nanostars, *ACS Infect. Dis.* 6 (2020) 947–953.
- [62] H.L. Zhou, Y.F. Liang, J.G. Zhang, F. Wang, Detection of benzylpenicillin sodium and ampicillin residue based on flower-like silver nanostructures using surface-enhanced Raman spectroscopy, *Res. Chem. Intermed.* 48 (2022) 117–128.
- [63] Y. Wang, H.C. Chen, L. Jiang, A highly reproducible SERS sensor based on an Au nanoparticles/graphene oxide hybrid nanocomposite for label-free quantitative detection of antibiotics, *Analyst* 146 (2021) 5740–5746.
- [64] R.C. Lora, L. Silveira, S.R. Zamuner, M.T.T. Pacheco, Dispersive Raman spectroscopy for the <i>in vitro</i> identification and quantification of injected vancomycin intra-vitreous, *Spectroscopy-Biomed. Appl.* 25 (2011) 103–112.
- [65] A. Dwivedi, O. Ryabchykov, C. Liu, E. Farnesi, M.S. Schmidt, T. Bocklitz, J. Popp, D. Cialla-May, SERS-driven ceftriaxone detection in blood plasma: a protein precipitation approach, *Chemosensors* 12 (2024).